Int. J. Electrochem. Sci., 16 **(2021)** Article ID: 210835, doi: 10.20964/2021.08.16

International Journal of
ELECTROCHEMICAL
SCIENCE
www.electrochemsci.org

Pore Scale Study of Dynamic Adsorption Process in Capacitive deionization Porous Electrode Based on Lattice Boltzmann Method

Shouguang Yao[*], *Xi Ding, Yi Ji, Xin Kan, Rui Liu*

School of Energy and Power Engineering, Jiangsu University of Science and Technology, 212003, Zhenjiang, Jiangsu, China
[*]E-mail: zjyaosg@126.com

Received: 2 April 2021 / *Accepted:* 26 May 2021 / *Published:* 30 June 2021

Capacitive deionization (CDI) has become a promising desalination technology due to its low energy consumption and environmental friendliness. Understanding the transport mechanism of ions within CDI porous electrodes is essential to improve desalination performance. In this study, a numerical model coupled with the Navier-Stokes equations, the concentration-diffusion equation, and the Langmuir isothermal adsorption equation is developed for the first time to describe the transport process in a porous electrode. To facilitate the calculations, a simplified particle model is used to describe the distribution of the particles in the porous electrode. With the discrete solution of the numerical model by means of the Lattice Boltzmann method, the transient changes of Na, Cl ion concentrations in the solution and the particles are accurately described. Using this numerical model, the effects of inlet solution velocity, electrode porosity and porous skeleton particle size on the internal mass transfer and adsorption performance of the CDI porous electrode were investigated at the pore scale. The results show that an appropriate increase in the inlet solution flow rate can effectively improve the adsorption amount and rate of the porous electrode. The increase of porosity improves the utilization rate and the average adsorption capacity of the electrode material. Decreasing the particle size of porous skeleton particles can reduce the internal mass transfer resistance of the porous electrode and enhance the adsorption performance of the electrode. This study shows that pore-scale simulations can help to understand the ion transport and adsorption mechanisms in capacitive deionization electrode particles and point the way for the next optimization.

Keywords: Capacitive deionization, Porous electrode, Langmuir, Lattice Boltzmann method, Pore-scale

1. INTRODUCTION

Capacitance deionization (CDI) is a new technology that can rapidly remove charged ions from the salt solution. Because of its low operating cost, friendly environment and high desalination

efficiency, CDI has attracted more and more attention in recent years [1-5]. The technique makes a salt solution to flow through a channel consisting of a pair of charged electrodes，the cation and anion in the solution move towards the cathode and anode respectively, and the ions are adsorbed and stored in the pores of the porous electrode[6-8]. In order to improve the ion adsorbed and storage capacity of the CDI unit, CDI electrodes usually use porous carbon materials with larger specific surface area, such as activated carbon, carbon aerogels, carbon fibers and carbon nanotubes. [9-12].

In order to explore the transport and adsorption characteristics of ions in CDI porous electrode, many scholars have established various models to describe the adsorption process of ions in electric double layers (EDL) on the electrodes surface, including the Gouy-Chapman-stern model [13], modified Donna model [14,15], and improved modified Donna model [16]. Although these complex models can describe the detailed characteristics of the system, but there is a simpler model, the Langmuir isotherm adsorption model, which can accurately describe the ion adsorption characteristics of CDI, and it is widely used in the study of CDI adsorption performance. Li[17] fabricated carbon nanotube and nanofiber composite film electrode for the electrosorption of Na^+ at various temperatures (281K-295K) and applied 1.2V DC voltage. With the increase of temperature, the removal rate of salt decreased from 45.4% to 33%. Langmuir isotherm was found to describe the experimental data better than Freundlich isotherm through the analysis of the electrosorption isotherm. In addition, the kinetics of electro adsorption accords with the first-order model, and the thermodynamic analysis shows that the CDI process is physical adsorption. Langmuir isotherm adsorption model is also used to study the selective adsorption of differently charged ions in solution by active carbon electrode [18] and the influence of different pore structure of activated carbon electrode on its adsorption performance[19]. Furthermore, some scholars have developed the Langmuir isotherm adsorption model to study the theory and numerical simulation of CDI adsorption. Johan Nordstrand[20] established a dynamic Langmuir adsorption model. They introduced charge concentration to simplify the classical Langmuir model. By comparing with the experimental data in a mass of literature, it is proved that the model can describe and predict the charge storage, ion adsorption and charging efficiency of CDI electrodes under different input ion concentrations, applied voltage and electrolyte composition. Yao [21] carried out the numerical simulation of multiple physical fields in CDI unit, and studied the adsorption law in CDI unit with the isothermal adsorption model as the verification. The above experimental and numerical simulation studies show that the desalting process of CDI system conforms to the Langmuir isotherm adsorption model. Through the experimental and theoretical analysis based on the Langmuir model, the influence of macro factors such as temperature, solution concentration, electrode material and pore structure on the adsorption performance can be obtained, and the macro characteristics such as selective adsorption of different ions and charge efficiency of CDI process can be analyzed. However, it is difficult to investigate the ion transport and adsorption properties from the experimental and macroscopic numerical simulations inside the electrode porous structure, which makes the understanding of the mechanism of adsorption and desorption inside the electrode pores and the influence mechanism of the porous structure, which are crucial to the desalination performance of CDI, still insufficient.

The lattice Boltzmann method (LBM) has a significant advantage in dealing with the ion transport process and complex boundary in the complex porous structure. Zhou [22] constructed a simple block porous structure based on the LBM method. Taking Langmuir model as the adsorption boundary,

the adsorption process of gas-solid in porous media was simulated at the pore scale, and the influence of flow conditions, porosity and adsorbent particle size on the whole dynamic adsorption performance was investigated. Afterward, Zhou [23] used the LBM to study the gas-solid adsorption process of porous media with random structure. A boundary recognition and classification method were proposed to identify and classify the porous interface nodes, and the influence of different pore structures on the adsorption energy was discussed in detail. Moreover, LBM has also been applied to the study of ion transport in electrochemical porous electrodes. Chen [24,25] explored the reaction transport phenomenon in PEMFC. Yang [26,27] studied the ion diffusion-reaction process in the charged porous structure at the pore scale. Since CDI is a physical adsorption process and is directed to charged ions in solution, the adsorption characteristics of CDI porous electrodes are different from the above studies on electrochemical and gas adsorption. At present, the only paper that combines the LBM method for ion transport and adsorption studies in CDI is a paper by Liu [28]. They investigated the dynamic ion transport and adsorption processes within CDI porous electrodes at the pore scale using the LBM method for the flow-through electrode (FTE) CDI.

As far as we know, the combination of the isothermal adsorption model and LBM has not been applied to the study of CDI adsorption characteristics. The combination of this model and LBM can provide a new perspective for CDI research. Aim at the negative electrode of the porous electrode of the flow-between electrode CDI unit, this paper constructs the two-dimensional skeleton digital model of the CDI porous electrode with a simplified structure. Using the LBM method, the Navier-Stokes equation, the concentration diffusion equation and the Langmuir adsorption model were coupled and solved to construct a simple LBM calculation model. Then, the dynamic mass transfer and adsorption process of the salt solution in the CDI porous electrode were simulated. The influence of the inlet velocity, porosity and particle size on the adsorption performance of the CDI porous electrode is investigated.

2. MODEL DESCRIPTION

2.1. Physical model

The structure diagram of the flow-between electrode CDI unit and porous electrode is shown in Fig. 1. When the system works, the direct-current power supply exerts a stable voltage on the CDI unit, and the salt solution flows through the channel between the charged electrodes to achieve the adsorption of ions in the salt solution.

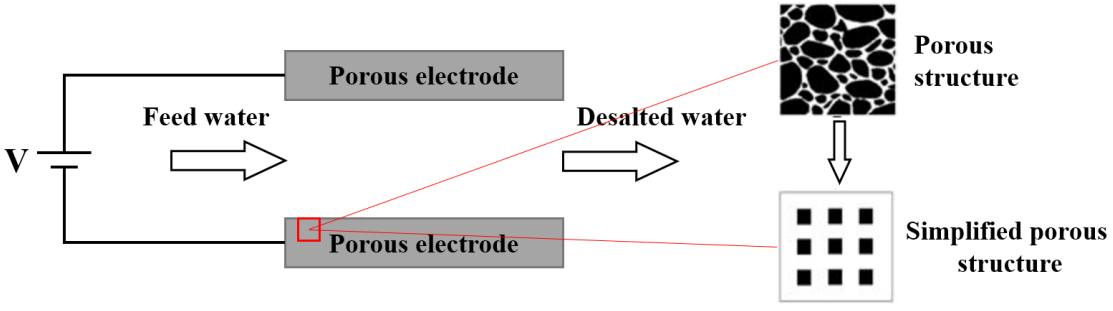

Figure 1. The structure diagram of flow-between electrode CDI unit and porous electrode.

In the direction perpendicular to the surface of the CDI negative electrode, the micro area of negative electrode and flow channel is selected to form the calculation area. In order to facilitate numerical research, the calculation area is simplified as the square area shown in Fig. 2. The upper and lower parts of the figure are the flow channel and the porous electrode, and the detailed dimensions are shown in Table. 1.

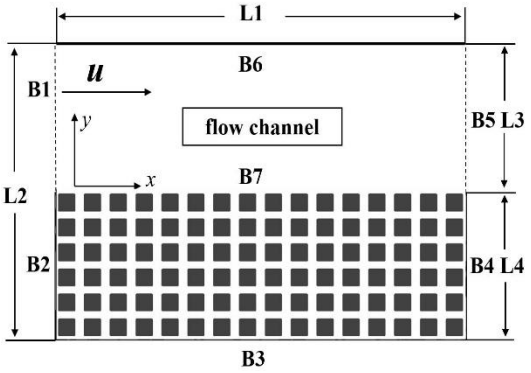

Figure 2. The two-dimensional physical model of the computational region.

Table 1. The detailed dimensions of the calculation area.

L1	L2	L3	L4
200μm	200μm	100μm	100μm

Square solid blocks were regarded as carbon particles. The length and number of blocks are defined as l_p and n, respectively. The block length can be regarded as the carbon particle size. Porosity ε refers to the pore area ratio to the total area of electrode area, as shown in the following formula.

$$\varepsilon = 1.0 - \frac{l_p \cdot n}{200 \times 100} \quad (1)$$

Porous electrodes with different structures are established as shown in Fig. 3. S1, S2 and S3 are structured with the same particle size and different porosity, while S4, S5 and S6 are structured with the same porosity and different particle size. Detailed parameters are shown in Table. 2.

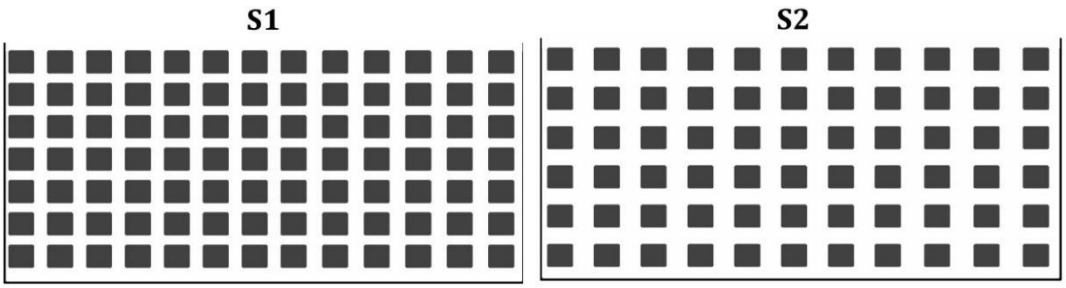

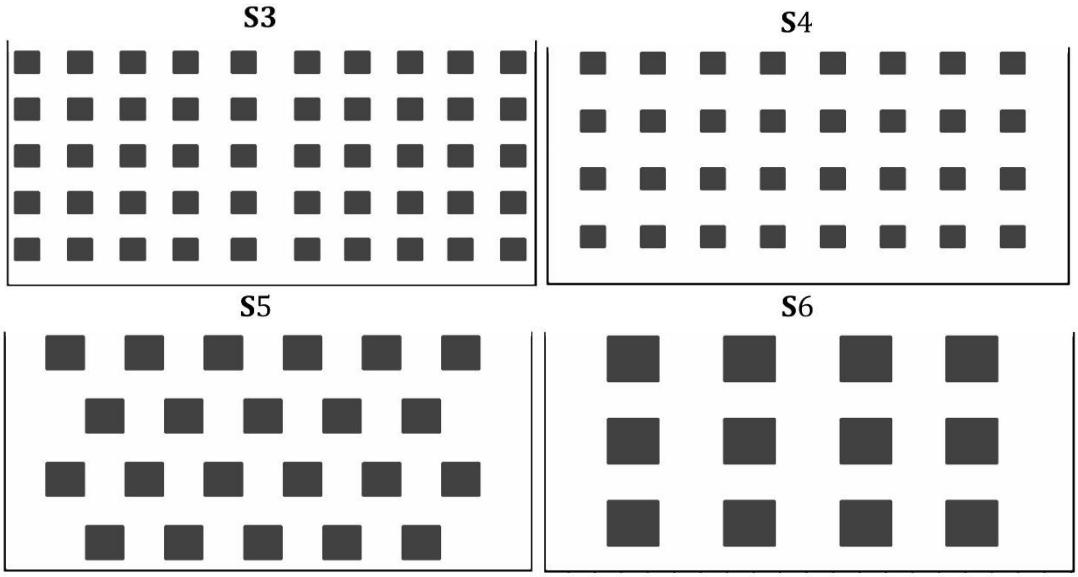

Figure 3. Porous electrodes of different structures.

Table 2. Features of porous electrodes structures.

结构	l_p(μm)	n	ε
S1	10	91	0.545
S2	10	66	0.67
S3	10	50	0.75
S4	10	32	0.84
S5	15	22	0.75
S6	20	12	0.75

2.2. Mathematical model

2.2.1. Governing equation for fluid flow

For the laminar flow and incompressible fluid flow in the flow channel, the governing equation is the Navier-Stokes equation:

$$\nabla \cdot \boldsymbol{u} = 0 \tag{2}$$

$$\frac{\partial \boldsymbol{u}}{\partial t} + \boldsymbol{u} \cdot \nabla \boldsymbol{u} = -\frac{\nabla p}{\rho} + \nu \cdot \nabla^2 \boldsymbol{u} \tag{3}$$

Where $\boldsymbol{u}$ is velocity vector; p is pressure; ρ is density; ν is kinetic viscosity.

2.2.2. Governing equation for concentration

Langmuir adsorption kinetics is used to describe the adsorption process on the surface of porous electrode particles. Then the concentration control equation and the boundary conditions of solid-liquid interface adsorption are as follows:

$$\frac{\partial C}{\partial t} = D\nabla^2 C - \boldsymbol{u}\cdot\nabla C \tag{4}$$

$$D\frac{\partial C}{\partial \boldsymbol{n}} = \frac{dq}{dt} = k_1 C\left(q_m - q\right) - k_2 q \tag{5}$$

Where C is the concentration of the solution; D is diffusivity; k_1 and k_2 are adsorption and desorption rates; q is the adsorbed amount; q_m is saturation adsorption amount.

2.2.3. Governing equation for mass transfer in particles

In the study of Matthew E. Suss [29], there are small nanoscale pores in the carbon particles of the porous electrode, so the absorbed ions will diffuse into the carbon particles. According to the homogeneous solid diffusion model (HSDM), the mass balance equation in the particle is written as:

$$\frac{\partial q}{\partial t} = D_s\nabla^2 q \tag{6}$$

Where D_s is solid diffusivity inside particles.

2.3. Lattice Boltzmann models

2.3.1. LBM for fluid flow

In this study, the LBGK collision model is selected for the fluid flow simulation and the lattice Boltzmann evolution equation can be described as follows:

$$f_i\left(\boldsymbol{X}+\boldsymbol{e}_i\Delta t, t+\Delta t\right) - f_i\left(\boldsymbol{X},t\right) = -\frac{1}{\tau_f}\left[f_i\left(\boldsymbol{X},t\right) - f_i^{eq}\left(\boldsymbol{X},t\right)\right] \tag{7}$$

Where f_i is the density distribution function at the lattice site $\boldsymbol{X}$ and time t; Δt is lattice time step; τ_f is dimensionless relaxation time; f_i^{eq} is the equilibrium distribution function; $\boldsymbol{e}_i$ is the discrete velocity. A D2Q9 lattice model is adopted in the current study for two-dimensional fluid flow simulations and $\boldsymbol{e}_i$ is given by:

$$\boldsymbol{e}_i = \begin{cases} (0,0) & & i=0 \\ \left(\cos\theta_i, \sin\theta_i\right) & \theta_i = (i-1)\pi/2 & i=1\sim 4 \\ \sqrt{2}\left(\cos\theta_i, \sin\theta_i\right) & \theta_i = (i-5)\pi/2+\pi/4 & i=5\sim 8 \end{cases} \tag{8}$$

The equilibrium distribution function is expressed as:

$$f_i^{eq}\left(X,t\right) = \rho w_i\left[1+\frac{3\boldsymbol{e}_i\cdot\boldsymbol{u}}{c_k^2}+\frac{9\left(\boldsymbol{e}_i\cdot\boldsymbol{u}\right)^2}{2c_2^4}-\frac{3\boldsymbol{u}^2}{2c_k^2}\right] \tag{9}$$

Where $c_k = \Delta x/\Delta t$ is the lattice speed; w_i is the weight coefficient with the value of $w_0 = 4/9$, $w_{1-4} = 1/9$, $w_{5-8} = 1/36$.

The macroscopic fluid density and velocity are as follows:

$$\rho = \sum_i f_i \tag{10}$$

$$\rho\boldsymbol{u} = \sum_i f_i\boldsymbol{e}_i \tag{11}$$

The relationship between relaxation time τ_f and kinetic viscosity ν is as follows:

$$\tau_f = \frac{3\nu}{\Delta x \cdot c_k} + 0.5 \tag{12}$$

2.3.2. LBM for mass transfer

The governing equation for concentration is a scalar transport equation, so the discrete velocity on the diagonal can be ignored, and the two-dimensional D2Q9 model can be simplified to D2Q5 model, which can improve the computational efficiency but not reduce the accuracy [30,31]. The evolution equation is as follows:

$$g_i\left(\boldsymbol{X}+\boldsymbol{e}_i\Delta t, t+\Delta t\right) - g_i\left(\boldsymbol{X},t\right) = -\frac{1}{\tau_g}\left[g_i\left(\boldsymbol{X},t\right) - g_i^{eq}\left(\boldsymbol{X},t\right)\right] \tag{13}$$

Where g_i is the concentration distribution function. The discrete velocity $\boldsymbol{e}_i$ of the D2Q5 model is given by:

$$\boldsymbol{e}_i = \begin{cases} (0,0) & i = 0 \\ \left(\cos\theta_i, \sin\theta_i\right) \quad \theta_i = (i-1)\pi/2 & i = 1 \sim 4 \end{cases} \tag{14}$$

The equilibrium concentration distribution function is expressed as:

$$g_i^{eq}\left(\boldsymbol{X},t\right) = Cw_i\left(1 + \frac{3\boldsymbol{e}_i \cdot \boldsymbol{u}}{c_k^2}\right) \tag{15}$$

Where w_i is the weight coefficient with the value of $w_i = 1/3$, $w_{1-4} = 1/6$ for D2Q5 model. The macroscopic concentration can be obtained from the following equation:

$$C = \sum_i g_i \tag{16}$$

The relationship between relaxation time τ_g and diffusivity D is as follows:

$$\tau_g = \frac{3D}{\Delta x \cdot c_k} + 0.5 \tag{17}$$

2.3.3. LBM for diffusion inside particles

The D2Q5 lattice model is still adopted for intra-particle diffusion, so the values of discrete velocity and weight factor are the same as those in the previous section. The evolution equation is as follows:

$$z_i\left(\boldsymbol{X}+\boldsymbol{e}_i\Delta t, t+\Delta t\right) - z_i\left(\boldsymbol{X},t\right) = -\frac{1}{\tau_z}\left[z_i\left(\boldsymbol{X},t\right) - z_i^{eq}\left(\boldsymbol{X},t\right)\right] \tag{18}$$

Where z_i is the concentration distribution function inside the particles; z_i^{eq} is the equilibrium distribution function of adsorption amount:

$$z_i^{eq}\left(\boldsymbol{X},t\right) = qw_i \tag{19}$$

The macroscopic adsorption amount can be obtained from the following equation:

$$q = \sum_i z_i \tag{20}$$

The relationship between relaxation time τ_z and solid diffusivity D_s is as follows:

$$\tau_z = \frac{3D_s}{\Delta x \cdot c_k} + 0.5 \tag{21}$$

2.4. Boundary conditions

As shown in Fig. 2, B1 is the inlet of the flow channel, where the velocity and concentration remain constant. B2 is the flush end of the porous electrode with the inlet of the flow channel, where there is no mass exchange with the outside, that is, the closed surface. B3 is the far flow channel side of the porous electrode, where the solution cannot continue to flow out, that is, the closed surface. B4 is the flush end of the porous electrode with the outlet of the flow channel, and its mass exchange with the outside area is ignored, that is, the closed surface. B5 is the outlet of the flow channel. B6 is the centerline of the solution channel, that is, the symmetrical boundary. B7 is the contact surface between the negative electrode of CDI and the salt solution in the flow channel.

The boundary conditions play a crucial role in the mass transfer system with the interface. The fluid boundary condition adopts the non-equilibrium bounce-back scheme proposed by Zou and He [32]. The concentration boundary condition adopts the boundary model proposed by Kang [33] to control the mass conservation of solute strictly. According to the corresponding concentration and its gradient, the concentration distribution function can be obtained by:

$$\sum_i g_i \boldsymbol{e}_i = C\boldsymbol{u} - D\nabla C \tag{22}$$

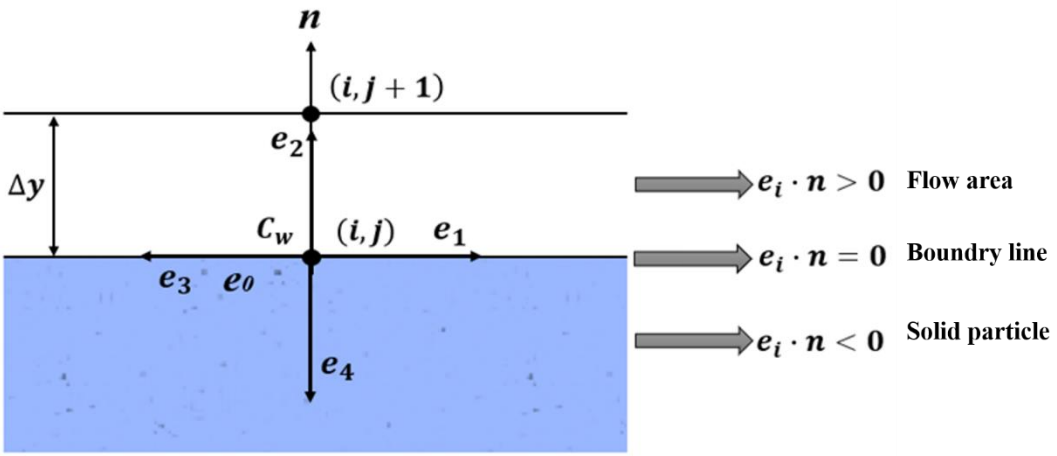

Figure 4. Schematic diagram of concentration distribution functions on a fluid-solid boundary.

Fig. 4 illustrates the concentration distribution function at the fluid-solid boundary node in the D2Q5 model. In the figure, the point (i, j) is the boundary node on the surface of solid particles; the point $(i, j+1)$ is the node in the fluid, and $\boldsymbol{n}$ is the normal vector at the boundary. Besides, the concentration distribution functions g_i at the boundary line and inside the particle are derived from the

streaming process of adjacent fluid nodes. The unknown distribution function in Fig. 4 is g_2, according to Eq. (22), and it can be expressed as:

$$g_2 = g_4 - D\frac{\partial C_w}{\partial y} \tag{23}$$

3. ADSORPTION SIMULATION IN POROUS ELECTRODE

At each time step, the simulation process was implemented in the order of the adsorption process, from the convection and diffusion of the salt solution to the adsorption on the outer surface of the porous electrode particles. The Navier-stokes equation, the concentration diffusion equation and the Langmuir adsorption model were coupled to obtain the adsorption amount of the electrode. Then, the adsorption amount at time $(t+1)$ can be obtained by:

$$q_{t+1} - q = \left[k_1 C(q_m - q) - k_2 q\right] \cdot \Delta t \tag{24}$$

In order to describe the overall adsorption performance of the porous structure, the sum of the adsorption amount $q_t(i, j)$ at time t calculated by LBM program of all nodes (i, j) is divided by the total number of calculated nodes to obtain the average adsorption amount $\bar{q}_t$, as shown in the following formula:

$$\bar{q}_t = \frac{\sum i \sum j q_t(i, j)}{N_{sum}} \tag{25}$$

Where N_{sum} is the total number of calculation nodes in the porous electrode; $\bar{q}_t$ is the average adsorption amount.

In order to obtain the values of adsorption and desorption rates, this paper refers to the study of Wang [19] on the capacitive deionization performance of high mesoporous activated carbon electrodes. Under the conditions of the initial concentration range of 150-500mg/L, temperature of 288k, 298K, 308k and voltage of 1.6V, respectively, they used Langmuir adsorption isotherm to fit the experimental data of porous electrode adsorbing NaCl. The results are shown in Table. 2. Langmuir adsorption isotherm is shown as follows:

$$q = \frac{q_m K_L C_e}{1 + K_L C_e} \tag{26}$$

Where $K_L = k_1 / k_2$ is the Langmuir adsorption equilibrium constant; C_e is the equilibrium concentration.

Table 3. Langmuir isotherm parameters and regression coefficients in Wang's study.

Isotherm	Model equation	Parameter	Value		
			288K	298K	308K
Langmuir	$q = \frac{q_m K_L C_e}{1 + K_L C_e}$	q_m	10.9	10.6	9.4
		K_L	0.057	0.102	0.130
		R^2	0.971	0.981	0.939

From Table. 2, the values of saturated adsorption amount q_m and adsorption equilibrium constant K_L at 298K are 10.6mg/g and 0.102, respectively. According to Eq. (24), when $t=1$, $q_0=0$, $q_1=k_1Cq_m$. It is known from the experimental study that the adsorption capacity q is always less than the saturated adsorption capacity q_m, so there is $k_1Cq_m<q_m$. Then k_1 is:

$$k_1<\frac{1}{C} \tag{27}$$

Due to the adsorption rate k_1 and desorption rate k_2 are parameters related to specific porous materials, and it is difficult to measure directly. In order to facilitate the numerical simulation, the equilibrium concentration of 500 mg/L is taken to calculate the adsorption rate k_1. Based on Eq. (27), we set $k_1=0.002$, then $k_2=0.0196$. In this paper, the adsorption process in the negative electrode of the CDI system is idealized as only Na^+ participates, and the molar mass of Na^+ is 23g/mol, so the saturated adsorption amount q_m is calculated to be 4.168mg/g.

The relevant physical parameters in the numerical simulation are shown in Table. 4:

Table 4. Relevant physical parameters.

Parameter	Physical symbol	Value	Unit
Domain length	L	200	μm
Solution density	ρ	1×10^3	$kg\cdot m^{-3}$
Kinetic viscosity	ν	1×10^{-6}	$m^2\cdot s^{-1}$
Inlet flow velocity	u_0	0.0597,0.1194,0.2985, 0.597,1.194,1.791	$m\cdot s^{-1}$
Inlet solution concentration	C_0	200	$mg\cdot L^{-1}$
Diffusivity of Na^+	D	1.96×10^{-8}	$m^2\cdot s^{-1}$
Solid diffusivity	D_s	3.82×10^{-11}	$m^2\cdot s^{-1}$
Electrode density	ρ_s	0.5	$g\cdot cm^{-3}$
Saturation adsorption amount	q_m	4.168	$mg\cdot g^{-1}$
Adsorption rate constant	k_1	0.002	$L\cdot mg^{-1}\cdot s^{-1}$
Desorption rate constant	k_2	0.0196	s^{-1}

3.1. Effect of fluid flow

In order to explore the effect of the inlet velocity of salt solution on the adsorption performance of porous electrode, different inlet velocities were selected, which were 0.0597m/s, 0.1194m/s, 0.2985m/s, 0.597m/s, 1.194m/s and 1.791m/s. Due to the similar trend of the electrodes with these structures at different inlet velocities, only one porous structure S3 (ε = 0.75) is selected for explanation.

The change of average adsorption amount with time at different inlet velocities is shown in Fig. 5. The average adsorption amount gradually increased from 0 to equilibrium state at different inlet velocities. The adsorption amount of porous electrodes increased rapidly in the first 50 μs, and then the rising trend gradually slowed down until equilibrium. Fig. 6 displays the relationship between the average adsorption amount, together with the time to reach the equilibrium state and the inlet velocity.

It can be seen from the figure that before the inlet velocity reaches a certain value, the adsorption capacity of the porous electrode increases with the increase of the inlet velocity. When the inlet velocity is 0.597m/s, the adsorption amount reaches the maximum value. However, as the inlet velocity continues to increase, the adsorption amount of the electrode decreases gradually. This happened because the higher the inlet velocity is under the same condition, the more ions will reach the surface of the electrode particles and be adsorbed. In this case, the porous electrode can reach the adsorption saturation state faster and improve its adsorption capacity. Nevertheless, when the velocity is too large, the contact time between the ions in the solution and the electrode surface is significantly shortened and the adsorption is insufficient, which results in the decrease of the adsorption capacity of the electrode. This trend is consistent with the conclusion of Zhao [34] on the study of the desalting performance of activated carbon coated electrodes. In addition, it can be seen from Fig. 6 that before the velocity increases to 0.597m/s, the time for adsorption to reach the equilibrium state decreases significantly. However, with the continuous increase of the inlet velocity, the downward trend tends to be gentle, that is, the effect of increasing the inlet velocity on the improvement of adsorption rate weakens. Therefore, appropriately increasing the inlet velocity can effectively improve the adsorption capacity and adsorption rate, while excessive inlet velocity will reduce the adsorption capacity of the electrode.

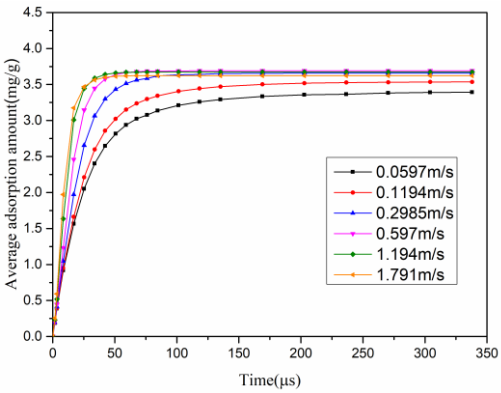

Figure 5. The relationship between the average adsorption capacity and time at different inlet velocities.

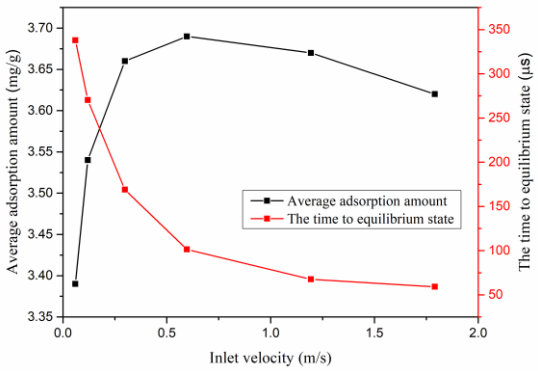

Figure 6. the relationship between the average adsorption amount, together with the time to reach the equilibrium state, and the inlet velocity.

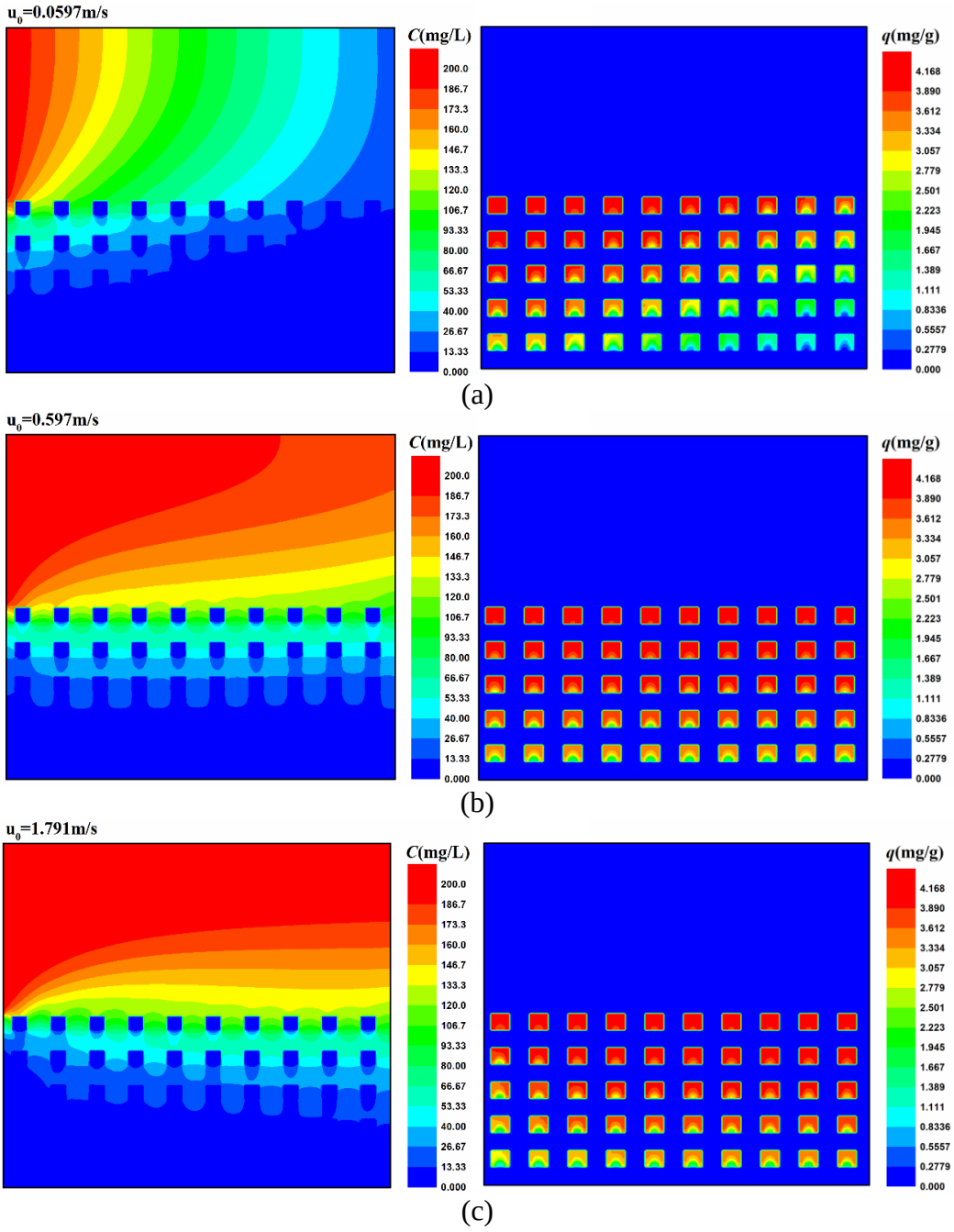

Figure 7. The distribution of ion concentration (left) and adsorption amount (right) in the porous electrode under different inlet velocities at 101 μs: (a) $u_0 = 0.0597\text{m/s}$, (b) $u_0 = 0.597\text{m/s}$, (c) $u_0 = 1.791\text{m/s}$.

Fig. 7 shows the distribution of ion concentration (left) and adsorption amount (right) in the porous electrode under different inlet velocities at 101 μs. From the comparison between Fig. 7 (a) and Fig. 7 (b), it can be seen that the larger the inlet velocity is, the more sufficient the concentration change in the fluid in the calculation domain is, and the adsorption in the electrode particles reaches saturation faster, which indicates that the proper increase of the inlet velocity promotes the mass transport between

the porous electrode particles and helps to improve the adsorption performance. Meanwhile, compared with Fig. 7 (b) and Fig. 7 (c), the concentration and adsorption amount at the end close to the inlet of the porous electrode in Fig. 7 (c) are significantly lower, which shows that the reduction of the adsorption amount of CDI porous electrode is mainly concentrated at the inlet. Therefore, in the practical design of the CDI unit structure, it is necessary to increase the residence time of salt solution in the CDI channel, especially at the inlet of the CDI unit.

3.2. Effect of porosity

In order to investigate the effect of different porosity of porous electrode on the dynamic adsorption process of CDI, the porous structure S1 (ε = 0.545), S2 (ε = 0.67), S3 (ε = 0.75) and S4 (ε = 0.84) with the same particle size and different porosity were selected, and the inlet velocity was 0.597m/s.

The average adsorption capacity $\bar{q}_t$ of different porous structures changes with time as shown in Fig. 8 (a). It can be seen from the figure that the smaller the porosity of the electrode, the smaller the average adsorption capacity of the porous electrode. The reason for this is that the smaller the porosity of porous media is, the closer its particle clusters are, so the more substantial the overlap of adsorption boundary effect is, which reduces the adsorption capacity. This is consistent with the research results of Liu [28] that the closer the particles are, the stronger the double layer overlap is, and the lower the adsorption capacity of CDI to ions. Further, it can be seen from figure 8 (b) that the time for electrodes with different porosity to reach adsorption equilibrium state is almost the same, which shows that under the same conditions, the change of porosity has little effect on the adsorption rate of CDI.

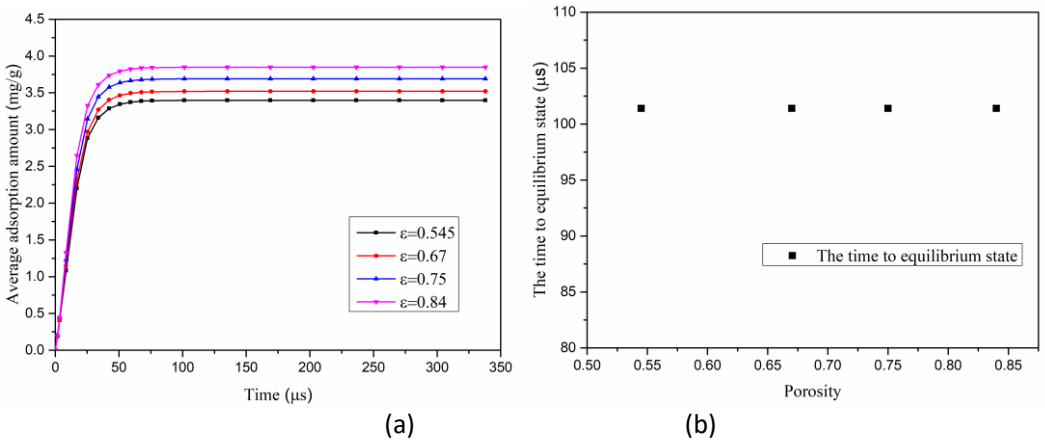

Figure 8. (a) The relationship between the average adsorption amount of porous electrodes with different porosity and time; (b) time for porous electrodes with different porosity to reach adsorption equilibrium state.

Fig. 9 describes the relationship between the overall adsorption amount and the average adsorption amount and porosity of porous electrodes in the adsorption equilibrium state. When other

factors are fixed, with the increase of porosity, the average adsorption amount of the porous electrode gradually increases, and it is closer to the saturated adsorption amount. However, the overall adsorption amount decreases along with the increase of porosity. Further, according to the distribution of adsorption amount in porous electrodes with different porosity under adsorption equilibrium state shown in Fig. 10, the distance between particles is more significant in the electrode with larger porosity, which leads to a more negligible mass transfer resistance between particles. Therefore, in an adsorption period, the particles in the porous electrode far away from the channel can absorb more ions, making the electrode more efficient. Moreover, the overall adsorption capacity of the porous electrode decreases with the increase of porosity, which owing to that when the size of the porous electrode is fixed, the increase of porosity makes the specific surface area of the porous electrode involved in the adsorption decrease, resulting in the decrease of the overall adsorption amount of the porous electrode. This shows that for the porous electrode with more significant porosity, although the adsorption performance of the electrode particles is stronger, the influence of porosity on the overall adsorption amount of the porous electrode should be considered. Therefore, in the practical design of CDI porous electrodes, the above two factors should be considered in the value of electrode porosity.

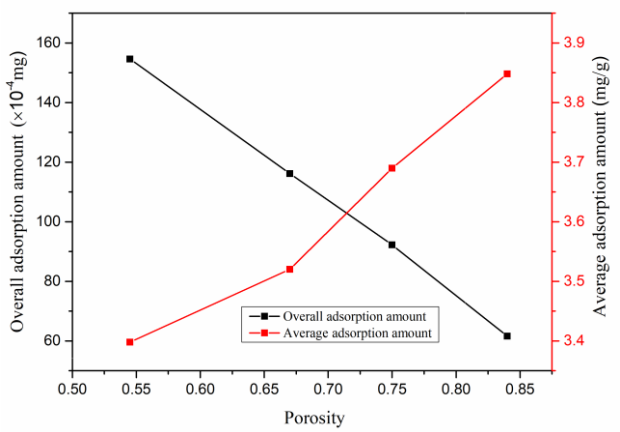

Figure 9. The relationship between overall adsorption amount, together with average adsorption amount, and porosity of porous electrode in adsorption equilibrium state.

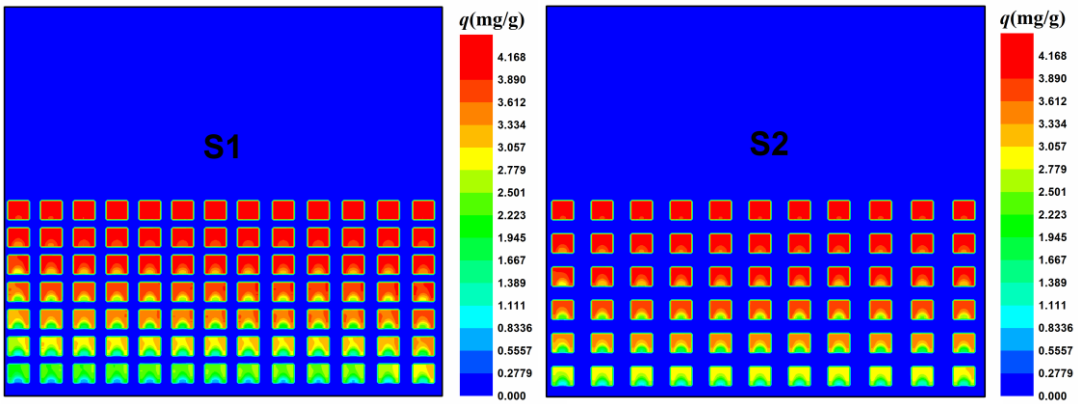

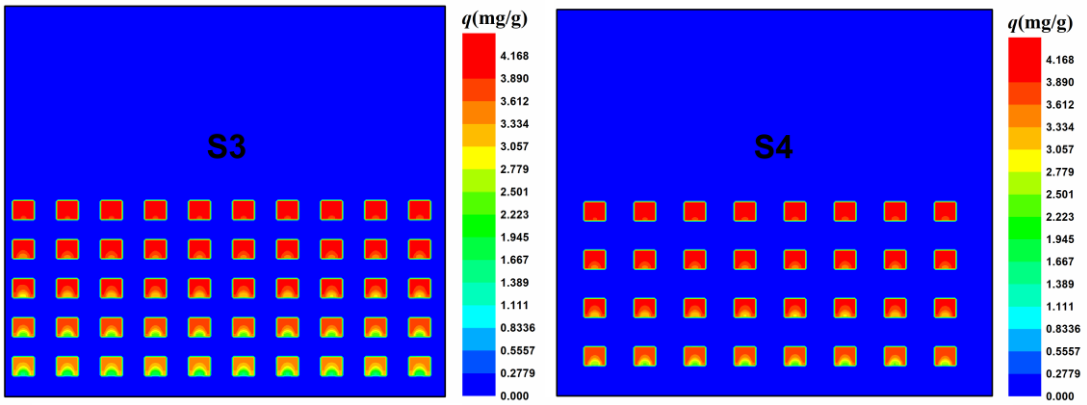

Figure 10. When the inlet velocity is 0.597m/s, the distribution of adsorption amount in porous electrodes with different porosity under adsorption equilibrium state.

3.3. Effect of particle size

To study the effect of different particle size of the porous electrode on the dynamic adsorption process of CDI, the porous electrodes with the same porosity (ε = 0.75), different particle size (S3 (*lp* = 10), S5 (*lp* =15) and S6 (*lp* =20) were selected, and the inlet velocity was 0.597m/s.

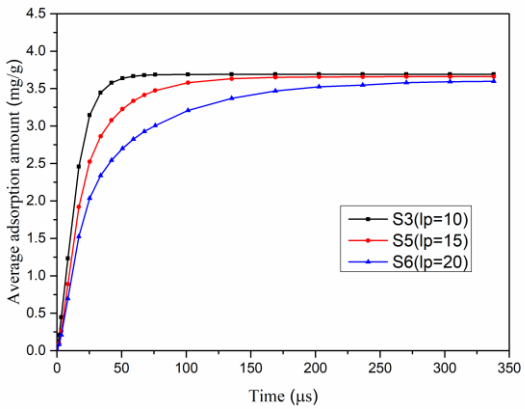

Figure 11. The relationship between the average adsorption amount of three porous electrodes (S3, S4, S5) and time.

Fig. 11 presents the change of the average adsorption amount of three porous electrodes with time. These curves show that the smaller the particle size is, the faster the average adsorption amount increases. Fig. 12 displays the relationship between the adsorption capacity, together with the time to reach the adsorption equilibrium state, and the particle size. It can be seen from the figure that with the increase of the particle size of the electrode, the time to reach the adsorption equilibrium increases significantly, while the adsorption amount decreases slightly. Furthermore, according to the distribution of adsorption amount in porous electrodes (S3, S5, S6) with different particle sizes in Fig. 13, the mass transfer resistance is more extensive in the particles with larger sizes, resulting in more time to reach the adsorption equilibrium state. Moreover, when the external size and porosity of the electrode stay

constant, the larger the particle size is, the lower the specific surface area is, and the weaker the adsorption capacity of the electrode is. Therefore, in order to obtain CDI porous electrode with high adsorption performance, materials with small particle size and large specific surface area should be selected.

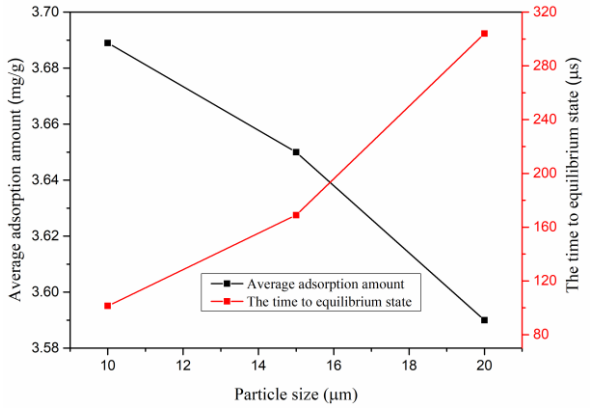

Figure 12. The relationship between adsorption capacity in equilibrium, together with and time to reach an adsorption equilibrium state, and particle size.

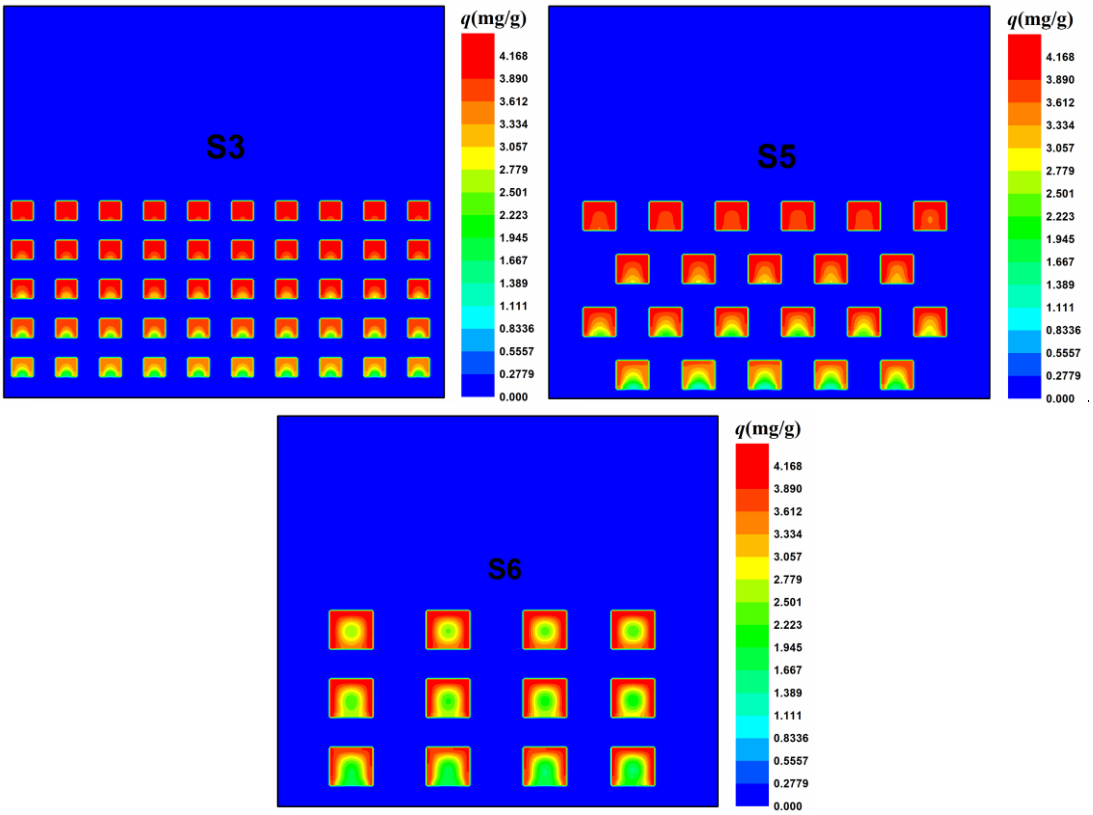

Figure 13. The distribution of adsorption amount of porous electrodes (S3, S5, S6) with different particle sizes in adsorption equilibrium state at the inlet velocity of 0.597m/s.

4. CONCLUSIONS

In the current paper, a dynamic mass transfer and adsorption model coupled with the Navier-Stokes equation, concentration diffusion equation, and Langmuir isothermal adsorption equation has been established by numerical simulation of the interior of porous capacitive deionization (CDI) electrode used for seawater desalination. Firstly, a two-dimensional skeleton model of the CDI porous electrodes with different structures was constructed using simplified particles. The above numerical model is discretized using the LBM method, and the solution flow rate and ion concentration distributions inside the porous electrodes are solved. Next, the mass transfer mechanisms inside the CDI porous electrode were investigated in terms of both operating parameters and particle structures.

In terms of operating parameters, the effect of inlet flow rate on the adsorption performance was investigated. The results show that the inlet velocity has a strong influence on the mass transfer and adsorption performance of the porous electrode. An appropriate increase in the inlet velocity can effectively enhance the adsorption capacity and rate. In contrast, an excessive inlet velocity will reduce the adsorption capacity of the electrode. The actual design of the CDI cell structure should try to increase the residence time of the solution at the inlet.

In terms of the particle structure, the effects of electrode porosity and porous skeleton particle size on the adsorption performance were investigated. The results showed that the variation of porosity had almost no effect on the adsorption rate of the porous electrodes but had a significant effect on the adsorption amount of the electrode. The increase of porosity is beneficial to increase the average adsorption capacity of the porous electrode, that is, to improve the utilization rate of the electrode material, but it will decrease the specific surface area of the electrode participating in the adsorption process so that the total adsorption capacity of the electrode will decrease. The particle size of the porous electrode has a direct effect on the internal mass transfer resistance of the particles. The larger the particle size, the more excellent the internal mass transfer resistance, which makes the adsorption take more time to reach the equilibrium state and reduces the adsorption rate of the porous electrode. Moreover, too large particle size will decrease the adsorption amount and reduce the adsorption performance of the electrode. Therefore, the porous electrode with a relatively small particle size is more favourable to improve the adsorption performance of the CDI system.

To the best of our knowledge, this is the first study that combines the Langmuir isothermal adsorption equation and the LBM method to study the mass transfer and transport mechanism inside a CDI porous electrode. This study is important because it helps to understand the influence of mass transfer and transport mechanisms on desalination performance and proposes optimized mechanism structures and operating parameters to improve the desalination capacity and rate. The ion transport mechanisms inside the porous electrodes under the influence of potential field are the emphasis of future research in our group.

ACKNOWLEDGEMENTS

This research was funded by the National Natural Science Foundation of China (Grant No. 51906091 and 51176092), and by Natural Science Research of Jiangsu Higher Education Institutions of China (Grant No. 19KJB470019).

References

1. Y. Liu, X. Gao, L. Zhang, X.L. Shen, X. Du, X.Y. Dou, X. Yuan, *Desalination.*, 494 (2020) 114665.
2. H. Deng, X.F. Chen, Y.Y. Tan, Y.Y. Liao, L. Yao, L.B. Deng, *Int. J. Electrochem. Sc*., 16 (2020) 210231.
3. T.M. Mubita, S. Porada, P.M. Biesheuvel, *Electrochim. Acta.*, 270 (2018) 165.
4. D.C. Han, C.M. Zhang, J. Guan, L.H. Gai, R.Y. Yue, L.N. Liu, M.Z. Afzal, C.Song, S.G. Wang, X.F. Sun , *Electrochim. Acta*, 336 (2020) 135639.
5. N. Deka, J. Barman, S. Kasthuri, V. Nutalapati, G.K. Dutta, *Appl. Surf. Sci.*, 511 (2020) 145576.
6. S. Porada, R. Zhao, A. V. D. Wal, *Prog. Mater. Sci*., 58 (2013) 1388.
7. X.B. Min, X.X. Hu, X.Y. Li, H.Y Wang, W.C. Yang, *J. Colloid. Interf. Sci*., 550 (2019) 147.
8. F. A. A. Marzooqi, A. A. A. Ghaferi, I. Saadat, *Desalination.*, 342 (2014) 3.
9. O. Sufiani, H. Tanaka, K. Teshima, R.L. Machunda, Y. A.C. Jande, *Sep. Purif. Technol*., 247 (2020) 116998.
10. J.M. Sun, Y.S. Liu, Z.W. Wu, M.C. Xu, L. E, C.H. Ma, S. Luo, J. Huang, W. Li, S.X. Liu, *Carbohyd. Polym*., 252 (2021) 117209
11. W.Q. Kong, G. Wang, M. Zhang, X.D. Duan, J.W. Hu, X.F. Duan, *Desalination.,* 459 (2019) 1.
12. P.F. Nie, J.B. Yan, G.D. Zhu, J.Y. Liu, *Electrochim. Acta.*, 339 (2020) 135920.
13. J. Gabitto, C. Tsouris, *Transp. Porous. Media.*, 109 (2015) 61.
14. M.E. Suss, P.M. Biesheuvel, T.F. Baumann, *Environ. Sci. Technol*., 48 (2014) 2008.
15. E.N. Guyes,A.N. Shocron, A. Simanovski, P.M. Biesheuvel, M.E. Suss, *Desalination.*, 415 (2017) 8.
16. S.D. Datar, K. Mohanapriya, D.J. Ahirrao, N. Jha, *Sep. Purif. Technol*., 257 (2021) 117972.
17. H.B. Li, L.K. Pan, *Chem. Phys. Lett*., 485 (2010) 161.
18. S.Y. Huang, C.S. Fan, C.H. Hou, *J. Hzard. Mater*., 278 (2014) 8.
19. G. Wang, B.Q. Qian, Q. Dong, *Sep. Purif. Technol*., 103 (2013) 216.
20. J. Nordstrand, J. Dutta, *J. Phys. Chem. C*., 123 (2019) 16479.
21. S.G. Yao, J.W. Wu, *Desalin. Water. Treat*., 144 (2019) 1.
22. L. Zhou, Z.G. Qu, *J. Comput. Phys*., 300 (2015) 800.
23. L. Zhou, Z.G. Qu, *Phys. Rev. E*., 93 (2016) 1.
24. R.Y. Zhang, T. Min, L. Chen, Q.j. Kang, Y.L. He, W.Q. Tao, *Appl. Energ*., 253 (2019) 113590.
25. L. Chen, R.Y. Zhang, P. He, *J. Power. Sources.*, 400 (2018) 114.
26. Y. Yang, M. Wang, *Cem. Concr. Compos*., 85 (2018) 92.
27. Y. Yang, M. Wang, *J. Colloid Interface Sci*., 514 (2018) 443.
28. R. Liu, S.G. Yao, *Int. J. Heat. Mass. Tran*., 135(2019) 769.
29. M. E. Suss, T.F. Baumann, W.L. Bourcier, *Energy. Environ. Sci*., 5 (2012) 9511.
30. S.P. Sullivan, F.M. Sani, M.L. Johns, *Chem. Eng. Sci*., 60 (2005) 3405.
31. L. Chen, Y.L. Feng, C.X. Song, *Int. J. Heat Mass Transf.*, 63 (2013) 268.
32. Q. Zou, X. He, *Phys. Fluids*., 9 (1997) 1591.
33. Q. Kang, P.C. Lichtner, D. Zhang, *Water. Resour. Res*., 43 (2007) 12.
34. Y. Zhao, X.M. Hu, S.L. Shan, *J. Safe. Enviro*., 12 (2012) 28.